Sodium/Iodide Symporter Mutant V270E Causes Stunted Growth but No Cognitive Deficiency

Juan Pablo Nicola, Andrea Reyna-Neyra, Paul Saenger, David F. Rodriguez-Buritica, José David Gamez Godoy, Radhika Muzumdar, L. Mario Amzel, and Nancy Carrasco

Department of Cellular and Molecular Physiology (J.P.N., A.R.-N., N.C.), Yale University School of Medicine, New Haven, Connecticut 06510; Department of Pediatrics (P.S., J.D.G.G.), Winthrop-University Hospital, Mineola, New York 11501; Department of Genetics (D.F.R.-B.), University of Alabama at Birmingham, Birmingham, Alabama 35294; Department of Pediatrics (R.M.), Albert Einstein College of Medicine, Bronx, New York 10467; and Department of Biophysics and Biophysical Chemistry (L.M.A.), Johns Hopkins University School of Medicine, Baltimore, Maryland 21205

Context: Iodide (I^-), an essential constituent of the thyroid hormones, is actively accumulated in the thyroid by the Na^+/I^- symporter (NIS), a key plasma membrane protein encoded by the *slc5a5* gene. Mutations in *slc5a5* cause I^- transport defects (ITDs), autosomal-recessive disorders in which I^- accumulation is totally or partially impaired, leading to congenital hypothyroidism. The characterization of NIS mutants has yielded significant insights into the molecular mechanism of NIS.

Objective: This study aimed to determine the basis of a patient's ITD clinical phenotype, by sequencing her *slc5a5* gene.

Design: Genomic DNA was purified and the *slc5a5* gene sequence determined. Functional in vitro studies were performed to characterize the V270E NIS mutant.

Patient: The index patient was diagnosed with hypothyroidism with minimal radioiodide uptake in a normally located, although enlarged, thyroid gland.

Results: We identified a new NIS mutation: V270E. The patient had the compound heterozygous NIS mutation R124H/V270E. R124H NIS has been characterized previously. We show that V270E markedly reduces I^- uptake via a pronounced (but not total) impairment of the protein's plasma membrane targeting. Remarkably, V270E is intrinsically active. Therefore, a negative charge at position 270 interferes with NIS cell surface trafficking. The patient's minimal I^- uptake enabled sufficient thyroid hormone biosynthesis to prevent cognitive impairment.

Conclusions: A nonpolar residue at position 270, which all members of the SLC5A family have, is required for NIS plasma membrane targeting. **(*J Clin Endocrinol Metab* 100: E1353–E1361, 2015)**

Active I^- accumulation, the first step in thyroid hormone biosynthesis, is mediated by the Na^+/I^- symporter (NIS), an integral plasma membrane glycoprotein located on the basolateral surface of thyrocytes (1). NIS couples the inward movement of Na^+ down its electrochemical gradient to the inward movement of I^- against its electrochemical gradient (2). NIS is expressed not only in the thyroid but also in other tissues, including lactating breast, salivary glands, stomach, and small intestine (3–7). The human *slc5a5* gene, which encodes NIS, a 643 amino acid protein, is located on chromosome 19p12–13 and consists of 15 exons (8). Our experimentally tested secondary structure model for NIS predicts a protein with 13 transmembrane segments (TMSs), an extracellularly fac-

ISSN Print 0021-972X ISSN Online 1945-7197
Printed in USA

Received March 31, 2015. Accepted July 17, 2015.
First Published Online July 23, 2015

Abbreviations: ClO_4^-, perchlorate; FACS, flow cytometry; HA, hemagglutinin; IL, intracellular loop; ITD, I^- transport defect; MDCK-II, Madin-Darby canine kidney; MVs, membrane vesicles; NIS, Na^+/I^- symporter; TMS, transmembrane segment; vSGLT, *Vibrio parahaemolyticus* Na^+/galactose symporter; WT, wild type.

ing amino terminus, and an intracellularly facing carboxy terminus (9, 10) (Supplemental Table 1).

I^- transport defect (ITD) is an autosomal-recessive disorder characterized by the inability of the thyroid gland to actively accumulate I^-, which leads to dyshormonogenic congenital hypothyroidism (11). The diagnostic criteria for ITD include a variable degree of hypothyroidism and goiter, low to absent thyroid radioiodide uptake, and low I^- saliva-to-serum ratio (12). However, the clinical presentation of the resulting phenotypes varies from euthyroid to severe hypothyroidism (13). To date, fourteen different loss-of-function mutations in the *slc5a5* gene have been identified in patients with ITD (11, 14). The detailed molecular analysis of several ITD-causing NIS mutants has yielded key mechanistic information on NIS structure/function; in particular, residues have been identified that are critical for substrate binding, specificity, stoichiometry, and plasma membrane targeting (15–20).

Here, we report a novel compound heterozygous missense and loss-of-function mutations in the *slc5a5* gene as a cause of ITD in a pediatric patient with stunted growth but no cognitive deficiency. The maternal allele carries a T>A transversion at position +809 in exon 6 resulting in a Val-to-Glu substitution at residue 270 (V270E), whereas the paternal allele encodes the ITD-causing mutant R124H (13, 15). We show that V270E markedly reduces I^- uptake when the protein is heterologously expressed, because targeting of V270E NIS to the plasma membrane is severely impaired. Replacing V270 with Asp (V270D) resulted in intracellular retention, whereas V270Q NIS was targeted to the cell surface. Strikingly, membrane vesicles from V270E NIS-expressing cells transported as much I^- as membrane vesicles from wild-type (WT) NIS-expressing cells, indicating that V270E NIS itself is highly functional. Therefore, a negative charge at position 270 does not destabilize the protein but rather interferes with NIS cell surface trafficking. Our results suggest that a nonpolar residue at position 270 is required for NIS maturation and plasma membrane trafficking. Of note, all members of the SLC5A family have a nonpolar residue at the equivalent position.

Materials and Methods

Case report

The patient was a full-term girl born to healthy, nonconsanguineous Jamaican parents. On day 2, an abnormally high TSH level was detected by neonatal screening (494 mIU/L; cutoff < 20 mIU/L). However, upon reexamination at day 11, she was diagnosed euthyroid (TSH, 8.00 mIU/L [normal range, 0.44–8.80 mIU/L] T_4, 9.0 μg/dL [normal range, 7.2–15.6 μg/dL]) and no thyroid hyperplasia was evident. Normal growth was observed during the first years of life. At the age of 4 years, her height was 109 cm (+1.88 SD). However, at 7 years 3 months of age, her height was 117 cm (−3.0 SD) and her weight was 22 kg (mean SD). Radiographic analysis revealed a bone age of 3 years. Severe hypothyroidism was diagnosed: TSH, 446 mIU/L (normal range, 0.50–4.30 mIU/L); free T_4, 0.1 ng/dL (normal range, 0.9–1.6 ng/dL); T_4, 0.5 μg/dL (normal range, 5.6–14.9 μg/dL). Her serum thyroglobulin was high (> 3000 ng/mL [normal range, 2.0–35.0 ng/mL]), and T_4-binding globulin levels were normal, 25.2 μg/mL (normal range, 16.3–30.7 μg/mL). No autoantibodies against thyroglobulin or thyroid peroxidase were reported. Thyroid ultrasonography showed multinodular enlargement of the gland. Thyroid scintigraphy revealed reduced diffuse I^- uptake (5.4%) 24 hours after the oral administration of 100 μCi $^{123}I^-$ (normal range, 10–40%), and virtually no uptake in salivary glands and stomach, suggesting a diagnosis of ITD. Of note, the patient's hypothyroidism did not seem to affect her intellectual development: age-appropriate school performance was reported. Thyroid hormone supplementation was started immediately after diagnosis, with a daily dose of 75 μg of levothyroxine. Six weeks after treatment her TSH level was 4.36 mIU/L and her thyroglobulin level was 1668 ng/mL. Thyroglobulin levels continued to decrease, reaching 204 ng/mL after 15 months of treatment. At the age of 8 years 6 months her height was 131 cm (−0.5 SD).

No clinical history of hypothyroidism was reported in the family of the proband's parents. The patient's parents and maternal half sister were clinically and biochemically euthyroid. However, her younger sister, who also had normal development and stature (mean SD), when evaluated at 2 years 6 months of age, showed TSH, 4.36 mIU/L; free T_4, 0.8 ng/dL; T_4, 5.6 μg/dL; and thyroglobulin, 1668 ng/mL. After a genetic diagnosis, she began receiving 50 μg of levothyroxine to prevent development of overt hypothyroidism.

Genetic analysis

The genetic analysis was approved by the ethics committee of the Winthrop-University Hospital and performed under informed written consent of the subjects themselves or their guardians thereof in accordance with all ethical standards and protocols. Genomic DNA was extracted from peripheral blood mononuclear cells. All 15 exons of the *slc5a5* gene were examined by sequencing DNA segments amplified by PCR as described (14). Nucleotide sequences of all PCR-amplified exons were determined in both orientations in triplicate (Keck DNA Sequencing Facility, Yale University). The nucleotide position in the human NIS mRNA was designated according to reference sequence (GenBank accession No. NM_000453.2). The adenine of the ATG translation start codon was denoted as nucleotide +1. The described V270E mutation was not detected in 50 euthyroid unrelated control patients subjected to BsaAI restriction enzyme analysis (see BsaAI restriction enzyme analysis).

BsaAI restriction enzyme analysis

The WT NIS allele contains a BsaAI restriction site between nucleotides +805 and +810 in exon 6. The mutation V270E disrupted the BsaAI site. Exons 6 and 7 were coamplified by PCR with the intervening intron 6 and subjected to digestion with BsaAI (New England Biolabs). Digested products were visualized after electrophoresis in a 2% agarose gel containing ethidium bromide. BsaAI digestion of WT allele produced frag-

ments of 353 and 137 bp, whereas, when the V270E mutation was present, the 490-bp PCR product remained undigested.

Homology model and electrostatic surface

The possible effects of the amino acid substitutions at position 270 of NIS were analyzed using our NIS homology model (17) based on the 3D structure of the *Vibrio parahaemolyticus* Na^+/galactose symporter (vSGLT) (21), a bacterial homolog of human Na^+/glucose symporter 1 (SGLT1). The sequence identity between vSGLT and NIS is 27% over residues 50–476, and the homology between them is 58%. After careful sequence alignment, an initial model was built using the software MODELLER (22). Cycles of improvement in sequence alignment and model building yielded the final model. Conformers for the substitutions at position 270—introduced using the software PyMOL (DeLano Scientific)—were selected and adjusted manually. The electrostatic maps for WT and V270 E/K/R NIS were generated and drawn with PyMOL.

Site-directed mutagenesis

The hemagglutinin (HA)-tagged human NIS cDNA construct containing nucleotides +1 to +1,932 was cloned in pcDNA3.1 vector (Invitrogen) and the R124H HA-NIS mutant was generated as described (15) NIS substitutions at position 270 were generated by site-directed mutagenesis using QuikChange Site-Directed Mutagenesis Kit (Stratagene) as reported (23). All constructs were sequenced to verify specific nucleotide substitutions.

Cell culture and transfections

FRTL-5 cells (a line of rat-thyroid–derived cells) were grown in Ham's F-12 media (Life Technologies) supplemented with 5% calf serum (Life Technologies), 3.6 ng/mL cortisol, 5 μg/mL transferrin, 10 ng/mL glycyl-L-histydyl-L-lysine acetate, 10 ng/mL somatostatin, 10 μg/mL insulin, and 1 mU/mL TSH as reported (24).

Cos-7 and Madin-Darby canine kidney (MDCK-II) cells were cultured in DMEM media (Life Technologies) supplemented with 10% fetal bovine serum (Life Technologies) as described (17). MDCK-II cells expressing WT NIS were cultured as reported (25). Stable MDCK-II polyclonal populations expressing V270E NIS were selected and propagated in growth medium containing 1 g/L G418 (Life Technologies). Cos-7 cells were transfected with 4 μg plasmid/10-cm dish using Lipofectamine Reagent enhanced with Plus Reagent (Life Technologies). FRTL-5 and MDCK-II cells were transfected with 7 μg plasmid/10-cm dish using Lipofectamine 2000 (Life Technologies).

Iodide uptake

I^- transport assays were performed as described (26). Briefly, cells were incubated in Hank's balanced salt solution containing 10μM I^- supplemented with 50 μCi/μmol carrier-free $Na^{125}I$ (PerkinElmer) for 30 minutes at 37°C. NIS-mediated I^- uptake was assessed in the presence of 40μM perchlorate (ClO_4^-). Accumulated $^{125}I^-$ was extracted with ice-cold ethanol and then quantified in a Cobra II Gamma Counter (Packard Bioscience). The amount of DNA was determined by the diphenylamine method after trichloroacetic acid precipitation (27). I^- uptake was expressed as picomoles per μg DNA and standardized by NIS expression analyzed by flow cytometry (FACS) under permeabilized conditions.

Initial rates of I^- transport were determined as described (19). Cells were incubated for 2 minutes with 0.625–80μM I^- (50 μCi/μmol carrier-free $Na^{125}I$), maintaining a constant 140mM Na^+ concentration, and uptake activity was evaluated as above. Experimental data were analyzed using the equation $v = (V_{max} \times [I^-])/(K_m + [I^-])$ and fitted by nonlinear least squares using Gnuplot software (www.gnuplot.info). Background data obtained in nontransfected cells were subtracted.

Membrane vesicles were prepared from Cos-7 cells as described (28). Aliquots containing 100 μg of protein were incubated at room temperature with an equal volume of a solution containing 40μM I^- (50 μCi/μmol carrier-free $Na^{125}I$), 1mM $MgCl_2$, 10mM HEPES (pH 7.5), 2mM methimazole, and 200mM NaCl for 2 minutes. Reactions were quenched with 1mM Tris-HCl (pH 7.5), 250mM KCl, and 1mM methimazole followed by rapid filtration through wet 0.22-μm nitrocellulose filters (EMD Millipore). Radioactivity retained by membrane vesicles was determined as described above.

Flow cytometry

Paraformaldehyde-fixed cells were incubated in PBS containing 0.2% BSA for nonpermeabilized conditions or an additional 0.2% saponin for permeabilized conditions with 0.1 μg/mL anti-HA rat monoclonal antibody (Roche Applied Science). After washing, cells were incubated with phycoerythrin-conjugated goat antirat antibody (Life Technologies). The fluorescence of 10^4 cells per tube was assayed in a FACS Calibur flow cytometer (BD Bio-Sciences). Data were analyzed with FlowJo software (Tree Star).

Statistical analysis

Results are presented as the mean ± SE of values from three independent experiments. Statistical tests were performed using Prism 3.0 software (GraphPad Software). Multiple group analysis was carried out by one-way ANOVA and the Newman-Keuls multiple-comparisons post-hoc test. Differences were considered significant at $P < .05$.

Results

Identification of the compound heterozygous NIS mutation R124H/V270E

ITD was suspected in a Jamaican 7-year-old female patient on the basis of hypothyroidism (TSH, 446 mIU/L [normal range, 0.50–4.30 mIU/L], free T_4, 0.1 ng/dL [normal range, 0.9–1.6 ng/dL], T_4, 0.5 μg/dL [5.6–14.9 μg/dL]), nodular goiter, and reduced $^{123}I^-$ accumulation in a normally located thyroid gland, as well as in salivary glands and stomach. Sequencing of the patient's NIS cDNA revealed a previously unidentified heterozygous T>A transversion at nucleotide +809, located in exon 6, which results in a Glu instead of a Val at position 270 (Figure 1A). The patient also has a G>A transition at nucleotide +371, located in exon 2, which results in an Arg to His substitution at residue 124, a mutation previously reported in a newborn in France (13) (Figure 1B). Thus, the patient bears a compound heterozygous mutation R124H/V270E. Analysis of the proband's family

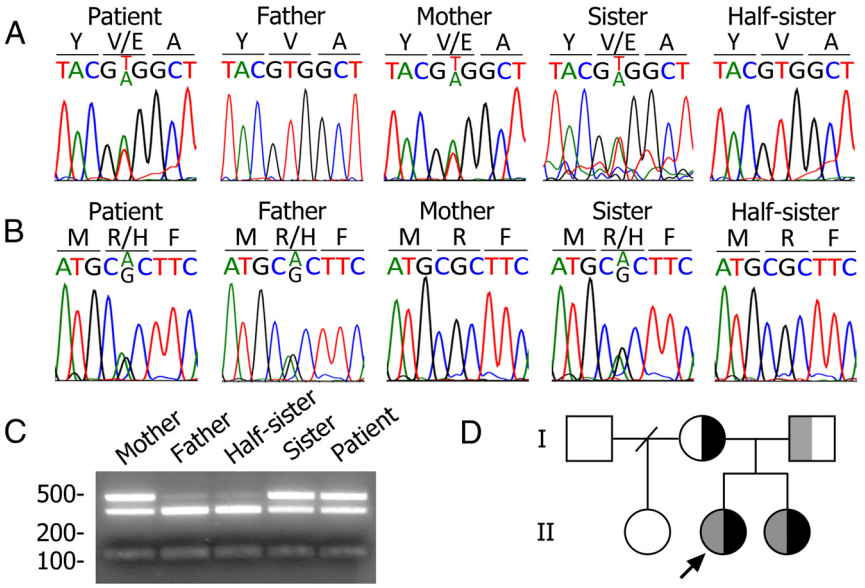

Figure 1. Identification of the compound heterozygous NIS mutation R124H/V270E. A, Chromatograms showing a 9-bp fragment of *slc5a5* exon 6 (nucleotides +805 to +813). Amino acids (Y269 to A271) are indicated using the one-letter code. The mother carries the mutation-bearing V270E allele. B, Chromatograms showing a 9-bp fragment of *slc5a5* exon 2 (nucleotides +367 to +375). The amino acid sequence (M123 to F125) is indicated using the one-letter code. The father carries the mutation-bearing R124H allele. C, BsaAI-restriction enzyme analysis. The 490-bp PCR product remains undigested in the presence of V270E. D, Pedigree analysis of the proband's family. The arrow indicates the propositus. The mutated alleles for V270E and R124H NIS are shown in black and gray, respectively.

showed that the mother is heterozygous for V270E NIS (Figure 1A) and the father for R124H NIS (Figure 1B). The parents' normal thyroid function is consistent with the recessive nature of ITDs. The same two mutations were present in the sister but not in the half sister (Figure 1, A and B). BsaAI restriction analysis demonstrated that the patient, her mother, and her sister were all heterozygous for V270E (Figure 1C). This information is summarized in a pedigree diagram (Figure 1D).

Mutant NIS proteins with charged residues at position 270 are minimally expressed at the plasma membrane, yet have the same apparent affinity for I^- as WT NIS

According to our NIS homology model (17) based on the crystal structure of the vSGLT (21)—a bacterial homolog of human SGLT1 (SLC5A1) and a member of the same family, the solute carrier 5 (SLC5) family, as NIS—R124 is located in intracellular loop 2 (IL-2), which connects transmembrane segments (TMSs) 3 and 4, and V270 at the end of TMS 7 (Figure 2A and Supplemental Figure 1). Molecular characterization of the R124H mutation uncovered the structural role of R124: to bridge IL-2 and IL-6. Based on this, we proposed an interaction between the δ-amino group of R124 (IL-2) and the thiol group of C440 (IL-6) (15). To determine the effect of the V270E substitution, Cos-7 cells, which do not express NIS endogenously, were transfected with WT or V270E NIS cDNAs. FACS analysis using an anti-HA antibody directed against an extracellular HA tag engineered onto the amino terminus of NIS (Supplemental Figure 1), in nonpermeabilized cells, showed that the levels of V270E NIS at the plasma membrane were significantly lower than those of WT NIS (Figure 2, B and C; surface). By contrast, FACS analysis under permeabilized conditions showed similar expression levels for both proteins (Figure 2, B and C; total). V270E NIS-expressing Cos-7 cells exhibited minimal I^- uptake, which was inhibited by perchlorate (ClO_4^-), a substrate of NIS (29) (Figure 2D). Furthermore, FRTL-5 cells (a line of highly functional rat thyroid–derived cells) transiently transfected to express WT, R124H, or V270E NIS and maintained without TSH to down-regulate their expression of endogenous NIS (30), displayed significantly lower R124H and V270E NIS levels at the plasma membrane than WT NIS-expressing cells, and consequently minimal-to-no NIS-mediated I^- accumulation (Supplemental Figure 2). Together, these findings suggest that the functional defect resulting from the V270E NIS mutation severely decreases targeting of NIS to the plasma membrane, and consequently reduces NIS-mediated I^- transport. On Western blots, the mature, fully glycosylated NIS polypeptide was barely detected in V270E NIS-expressing cells, indicating that this mutant protein was not fully processed; consistent with this observation, most of the V270E polypeptide was sensitive to Endo H, indicating that V270E is retained before it can reach the *medial*-Golgi (Supplemental Figure 3). This experiment was carried out in MDCK-II cells permanently expressing V270E or WT NIS to obtain better resolution, because NIS is expressed at lower levels and oligomerizes less in MDCK-II cells than in Cos-7 cells. The electrophoretic pattern of WT NIS, by contrast, showed a higher ratio of mature (~75–100 kDa) to Endo H-sensitive, partially glycosylated (~60 kDa) polypeptide, which has been observed previously (15, 16).

To ascertain whether the intracellular retention of V270E NIS was due to the negatively charged Glu, we replaced V270 with Asp or Gln. V270D NIS, like V270E, did not reach the plasma membrane efficiently; V270Q

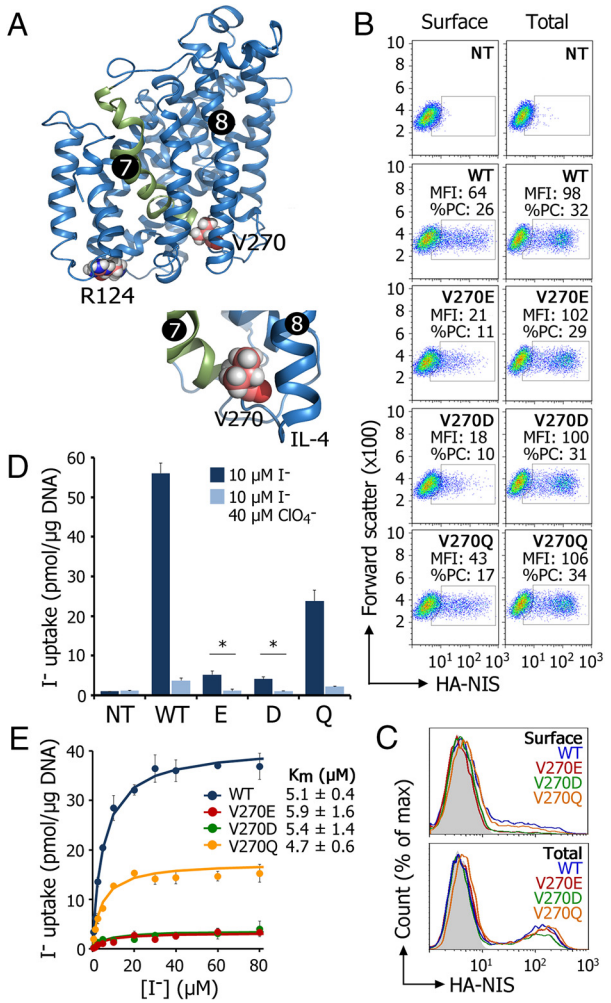

Figure 2. Negatively charged residues at position 270 markedly impair targeting of NIS to the plasma membrane. A, NIS homology model highlighting R124 and V270. TMS 7 is depicted in green. B, Representative FACS analysis (forward scatter vs. fluorescence intensity) of NIS expression in Cos-7 cells under nonpermeabilized (left panel; surface) and permeabilized (right panel; total) conditions. NT; nontransfected cells; WT, V270E, V270D, and V270Q: cells transfected with wild type, V270E, V270D, or V270Q NIS, respectively. MFI: median fluorescence intensity; %PC: percentage of transfected cells. C, Representative FACS analysis (histogram) of NIS expression in Cos-7 cells under nonpermeabilized (upper panel; surface) and permeabilized (lower panel; total) conditions. Nontransfected cells are represented in solid gray. D, Steady-state I^- uptake in Cos-7 cells, either nontransfected (NT) or transiently expressing WT or V270E/D/Q NIS. Cells were incubated with 10μM I^- in the absence (dark bars) or presence (light bars) of 40μM ClO_4^-. Results are expressed in pmol I^-/μg of DNA ± SD. *, $P < .05$ (ANOVA, Newman-Keuls test). E, Initial rates of I^- uptake were determined at the indicated concentrations of I^-. Calculated curves (smooth lines) were generated using the equation $v = (V_{max} \times [I^-])/(K_m + [I^-])$ adjusted to subtract out background data obtained from nontransfected cells. K_m values are indicated as mean ± SD (n = 3).

NIS, in contrast, did (Figure 2, B and C; surface). All mutants were expressed at similar levels (Figure 2, B and C; total). Furthermore, in steady-state I^- uptake assays, V270D NIS displayed modest I^- accumulation (Figure 2D). Interestingly, Gln at position 270 restored I^- transport, although not completely (Figure 2D). Initial rates of I^- transport showed that V270E, D, and Q NIS had virtually the same apparent affinity (K_m) for I^- as WT NIS. By contrast, the V_{max} values ranged from lower (V270Q) to markedly lower (V270E/D) than those of WT NIS (Figure 2E). In summary, a negatively charged residue at position 270 causes NIS to be retained intracellularly.

Experiments performed in Cos-7 cells transiently coexpressing V270E or R124H with WT NIS, mimicking a heterozygous state, suggested that the mutated allele does not interfere with the activity of WT NIS (Figure 3A). Moreover, coexpression of V270E and R124H did not increase I^- transport mediated by V270E (Figure 3A) or its targeting to the cell surface (Figure 3B).

V270E is intrinsically active

To determine the intrinsic activity of V270E NIS, we measured I^- transport in membrane vesicles (MVs) (ie, sealed sacs derived from all the membranous organelles except the nucleus) (31). Strikingly, MVs from Cos-7 cells expressing V270E NIS transported nearly as much I^- as MVs from cells expressing WT NIS (Figure 4A), indicating that although trafficking of V270E NIS to the cell surface is impaired, the protein itself is highly functional. This demonstrates that the negative charge of a Glu at position 270 does not affect NIS folding, stability, or activity; rather, the subtle change in the surface charge of the intracellularly facing domain (Figure 4B) may interfere with interacting proteins that are essential for trafficking NIS to the cell surface. These results stand in stark contrast with those obtained with other ITD-causing NIS mutants that, although completely inactive, do reach the cell surface (17–20).

Position 270 tolerates positively charged residues

To investigate the effect of positively charged residues at position 270, we engineered Arg and Lys at this position. FACS analysis under permeabilized conditions showed no difference in WT, V270K, or V270R NIS expression (Figure 5A; total). Under nonpermeabilized conditions, however, less V270K and R NIS were targeted to the plasma membrane than WT NIS (Figure 5A; surface). Remarkably, V270K and V270R NIS displayed some I^- uptake at steady state (Figure 5C). The K_m values for I^- of V270K and R were virtually identical to that of WT NIS (Figure 5D).

Neutral residues at position 270 partially or fully restore NIS cell surface expression

The neutral amino acids Ala, Ile, Leu, and Thr were individually placed at position 270. Each of the resulting NIS mutants was properly expressed and targeted to the

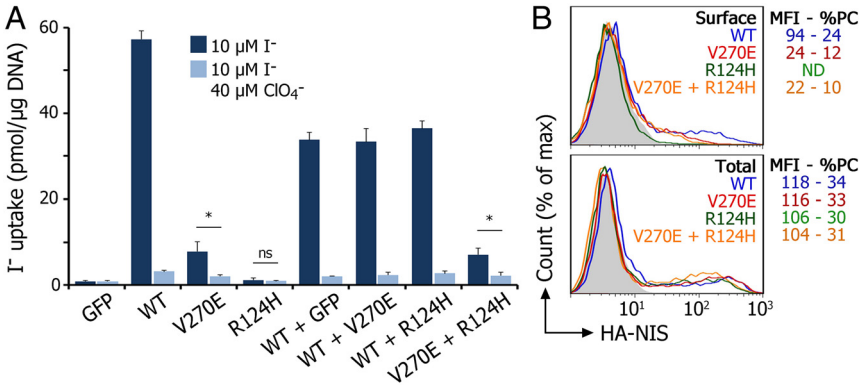

Figure 3. Neither R124H nor V270E NIS interferes with WT NIS activity when coexpressed with WT NIS. A, Steady-state I^- uptake in Cos-7 cells transiently transfected with the GFP-expressing vector pEGFP (Clontech), WT NIS, or one of the NIS mutants R124H and V270E (5 μg/10 cm dish). In WT/GFP-, WT/R124H-, WT/V270E-, and V270E/R124H-cotransfected cells, a half dose of each of the plasmids was used (2.5 μg/10 cm dish), to keep the total amount of DNA constant. Cells were incubated with 10μM I^- in the absence (dark bars) or presence (light bars) of 40μM ClO_4^-. Results are expressed in pmol I^-/μg of DNA ± SD. *, $P < .05$ (ANOVA, Newman-Keuls test). ns, nonstatistically significant. B, Representative FACS analysis of WT or mutant NIS expression under nonpermeabilized (upper panel; surface) and permeabilized (lower panel; total) conditions using anti-HA antibody. Cos-7 cells transiently transfected with HA-tagged WT NIS, HA-tagged R124H, HA-tagged V270E NIS, and HA-tagged V270E + nontagged R124H NIS (2.5 μg per mutant/10-cm dish). A vector encoding the Na^+/monocarboxylate transporter (SMCT) was added to adjust for equal amounts of transfected DNA.

cell surface (Figure 5B). These mutants transported I^- to significant, albeit varying, extents (Figure 5C). Ile at position 270 yielded a mutant that transported I^- at levels close to those of WT NIS; Ile, like Val, has a nonpolar side chain branched at the β-carbon. However, Thr, a polar amino acid branched at the β-carbon, did not fully restore NIS activity. Furthermore, the nonpolar residues Ala and Leu partially restored NIS function. Consistent with these observations, all members of the SLC5A family have a Leu or Ile at the position corresponding to V270 in NIS (Figure 5E). The apparent affinity for I^- of all these mutants is the same as that of WT NIS (Figure 5D). Normalizing the levels of I^- uptake in terms of the amount of WT or mutant NIS expressed at the plasma membrane revealed that the decrease in transport by mutant NIS results from impaired targeting to the plasma membrane, not from reduced intrinsic activity (Supplemental Figure 4).

Discussion

The ability of NIS to transport I^- at the submicromolar concentrations found in the bloodstream is remarkable given the difficulty of binding a halide ion such as I^- with high affinity (32). We have recently reported that NIS overcomes this problem by taking advantage of the physiological Na^+ concentration (~145mM) and the increase in affinity for the second Na^+ that occurs when the first Na^+ site is occupied. We have shown that, at the physiological Na^+ concentration, ~79% of NIS molecules are occupied by two Na^+ ions, and hence ready to bind and transport I^- (33). This property of NIS is particularly relevant to the case presented here because thyroid hormones are critical for the development of the fetal and neonatal brain, as well as the musculoskeletal system and lungs in the child (34). Thyroid hormone insufficiency at the beginning of life can lead to congenital hypothyroidism, which, depending on the severity of the hormone deficiency, may result in mental retardation and stunted growth. In the patient examined here, the evidence suggests that the small amount of V270E NIS that reached the plasma membrane mediated sufficient I^- uptake to permit the synthesis of enough thyroid hormones to ensure adequate cognitive development and linear growth during the initial 4 years of life, even though there was a marked growth stunt afterwards which was reversed after levothyroxine administration (Supplemental Figure 5).

Patients with ITDs bearing different NIS mutations have been shown to have a wide variety of clinical manifestations (13). The genotype-specific age of onset of hypothyroidism may depend on differences in residual mutant NIS activity across

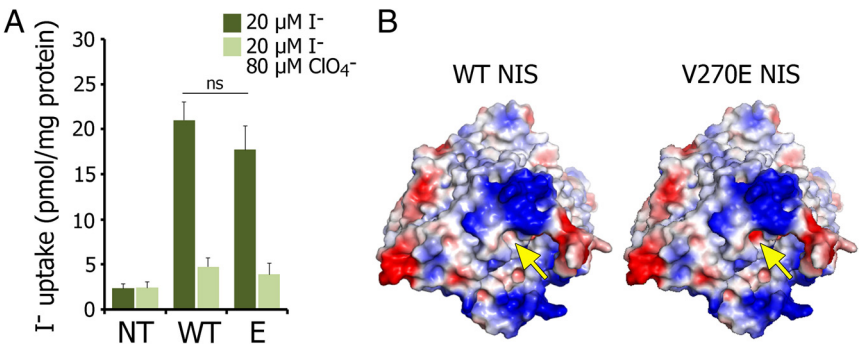

Figure 4. V270E NIS is intrinsically active. A, I^- uptake in membrane vesicles prepared from nontransfected (NT) or from WT- or V270E NIS-expressing Cos-7 cells. Membrane vesicles were incubated with 20μM I^- in the absence (dark bars) or presence (light bars) of 80μM ClO_4^-. Results are expressed as pmol I^-/mg protein ± SD. ns, nonstatistically significant. B, Electrostatic surface of WT and V270E NIS. The yellow arrow points to the location of residue 270 in NIS. The introduction of a glutamate increases the size of a negative patch at the surface of NIS close to the cytosolic region of the molecule. Positive and negative potentials are shown in blue and red, respectively. The surface was calculated and plotted using PyMOL software.

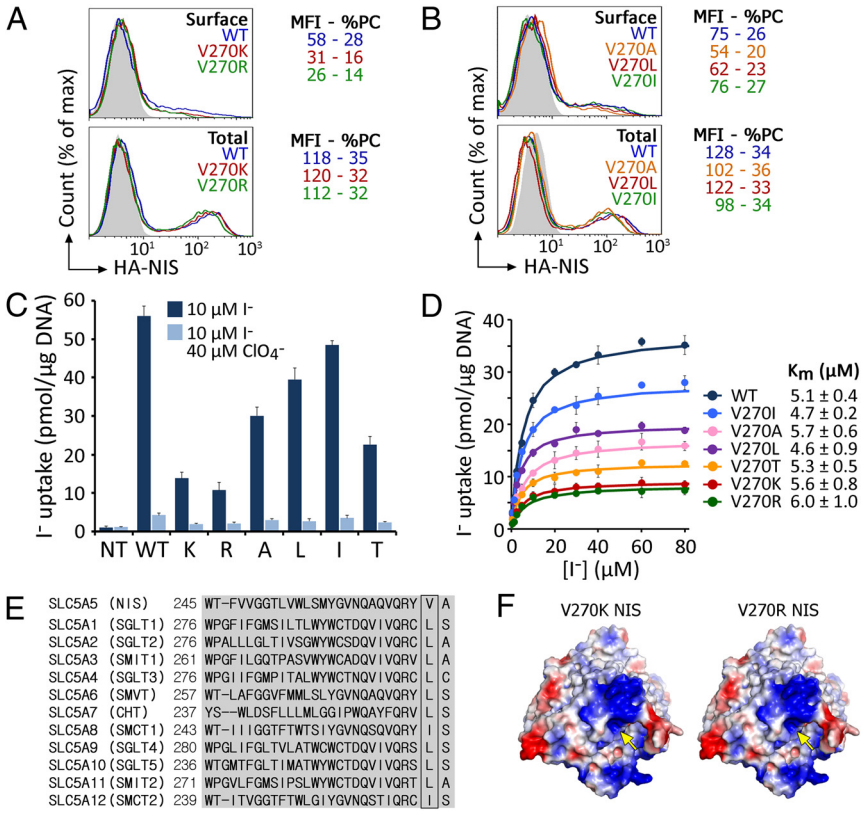

Figure 5. Neutral amino acids at position 270 rescue NIS plasma membrane targeting to different degrees. A and B, Representative FACS analysis of WT or mutant NIS expression in Cos-7 cells under nonpermeabilized (upper panel; surface) and permeabilized (lower panel; total) conditions. Nontransfected cells (NT) are represented in solid gray. MFI, median fluorescence intensity; %PC, percentage of transfected cells. C, Steady-state I^- uptake in Cos-7 cells either nontransfected (NT) or transiently expressing WT or V270K/R/A/L/I/T NIS. Results are expressed in pmol $I^-/\mu g$ of DNA ± SD. D, Initial rates of I^- uptake were determined at the indicated concentrations of I^-. K_m values are indicated as mean ± SD (n = 3). E, Alignment of the TMS 7 sequences of members of the human SLC5A family. V270 of SLC5A5 (NIS) is shown along with the corresponding residues in other members of the family. F, Electrostatic surface of V270R/K NIS. The yellow arrow points to the location of residue 270 in NIS. Positive and negative potentials are shown in blue and red, respectively. The surface was calculated and plotted using PyMOL software.

NIS gene defects. Our proband bearing the compound heterozygous mutation R124H/V270E developed clinical hypothyroidism in childhood. In sharp contrast, the ITD patient harboring a homozygous, fully intracellularly retained R124H mutant developed hypothyroidism with significant clinical manifestations as a neonate. This difference in the age of presentation may have been due to residual V270E NIS activity, an explanation compatible with the patient's reduced, although not absent, $^{123}I^-$ uptake, which was revealed by thyroid scintigraphy. In this context, the increase in TSH levels following a reduction in thyroid hormone production might have partially overcome the defect in trafficking of V270E NIS to the plasma membrane by enhancing NIS transcription, as occurred in patients with ITDs carrying the missense mutation T354P (35). Consistent with this possibility, the proband's high serum thyroglobulin levels suggest TSH-induced overstimulation of the thyroid tissue (36).

The mutant protein is intrinsically active (Figure 4A), but the additional negative charge imparted by the Glu at position 270 impairs its maturation and trafficking to the plasma membrane, resulting in markedly decreased I^- accumulation. The subtle change in the surface charge of a positive patch in the intracellularly facing domain of the NIS molecule (Figure 4B) may hinder interactions between NIS and proteins key for its trafficking to the cell surface. Consistent with this possibility, increasing the amount of positive charge in the patch by introducing Arg or Lys at position 270 (Figure 5F) partially restored plasma membrane targeting (Figure 5A). Unsurprisingly, when the original Val was replaced with Ile or even Leu, plasma membrane targeting was mostly retained (Figure 5B).

Trafficking is also compromised by missense mutations in other members of the SLC5 family, such as the Na^+/glucose symporters SGLT1 (encoded by *slc5a1*) and SGLT2 (encoded by *slc5a2*) (37). Autosomal-recessive mutations in *slc5a1* and *slc5a2* that result in the intracellular retention of SGLT1 and SGLT2 cause glucose-galactose malabsorption and renal glucosuria, respectively (37). Additional studies are needed to identify proteins that interact with NIS, to determine whether these proteins also interact with other members of the SLC5 family, and to eventually attempt to modulate their interactions.

Acknowledgments

We thank all the members of the Carrasco laboratory for providing technical assistance and for many helpful discussions. J.P.N. was supported by a Brown-Coxe postdoctoral fellowship from the Yale School of Medicine.

Address all correspondence and requests for reprints to: Nancy Carrasco, Department of Cellular and Molecular Physiology, Yale University School of Medicine, 333 Cedar Street, New Haven, CT 06510. E-mail: nancy.carrasco@yale.edu.

Present address of J.P.N., Departamento de Bioquímica Clínica, Facultad de Ciencias Químicas, Universidad Nacional de Córdoba, 5000 Córdoba, Argentina.

Present address of R.M., Division of Endocrinology, University of Pittsburgh School of Medicine, Pittsburgh, Pennsylvania 15224.

Present address of D.F.R.-B., Department of Pediatrics, University of Texas at Houston Medical Center, Houston, Houston, Texas 77030.

This work was supported by National Institutes of Health Grant DK-41544 (N.C.).

Disclosure Summary: The authors have nothing to disclose.

References

1. **Dai G, Levy O, Carrasco N.** Cloning and characterization of the thyroid iodide transporter. *Nature*. 1996;379:458–460.
2. **Carrasco N.** Iodide transport in the thyroid gland. *Biochim Biophys Acta*. 1993;1154:65–82.
3. **Wapnir IL, van de Rijn M, Nowels K, et al.** Immunohistochemical profile of the sodium/iodide symporter in thyroid, breast, and other carcinomas using high density tissue microarrays and conventional sections. *J Clin Endocrinol Metab*. 2003;88:1880–1888.
4. **Tazebay UH, Wapnir IL, Levy O, et al.** The mammary gland iodide transporter is expressed during lactation and in breast cancer. *Nat Med*. 2000;6:871–878.
5. **Altorjay A, Dohan O, Szilagyi A, Paroder M, Wapnir IL, Carrasco N.** Expression of the Na+/I- symporter (NIS) is markedly decreased or absent in gastric cancer and intestinal metaplastic mucosa of Barrett esophagus. *BMC Cancer*. 2007;7:5.
6. **Nicola JP, Reyna-Neyra A, Carrasco N, Masini-Repiso AM.** Dietary iodide controls its own absorption through post-transcriptional regulation of the intestinal Na+/I- symporter. *J Physiol*. 2012;590:6013–6026.
7. **Nicola JP, Carrasco N, Masini-Repiso AM.** Dietary I(-) absorption: expression and regulation of the Na(+)/I(-) symporter in the intestine. *Vitam Horm*. 2015;98:1–31.
8. **Smanik PA, Ryu KY, Theil KS, Mazzaferri EL, Jhiang SM.** Expression, exon-intron organization, and chromosome mapping of the human sodium iodide symporter. *Endocrinology*. 1997;138:3555–3558.
9. **Levy O, De la Vieja A, Ginter CS, Riedel C, Dai G, Carrasco N.** N-linked glycosylation of the thyroid Na+/I- symporter (NIS). Implications for its secondary structure model. *J Biol Chem*. 1998;273:22657–22663.
10. **Levy O, Dai G, Riedel C, et al.** Characterization of the thyroid Na+/I- symporter with an anti-COOH terminus antibody. *Proc Natl Acad Sci U S A*. 1997;94:5568–5573.
11. **Portulano C, Paroder-Belenitsky M, Carrasco N.** The Na+/I- symporter (NIS): Mechanism and medical impact. *Endocr Rev*. 2014;35:106–149.
12. **Wolff J.** Congenital goiter with defective iodide transport. *Endocr Rev*. 1983;4:240–254.
13. **Szinnai G, Kosugi S, Derrien C, et al.** Extending the clinical heterogeneity of iodide transport defect (ITD): A novel mutation R124H of the sodium/iodide symporter gene and review of genotype-phenotype correlations in ITD. *J Clin Endocrinol Metab*. 2006;91:1199–1204.
14. **Nicola JP, Nazar M, Serrano-Nascimento C, et al.** Iodide transport defect: Functional characterization of a novel mutation in the Na+/I- symporter 5'-untranslated region in a patient with congenital hypothyroidism. *J Clin Endocrinol Metab*. 2011;96:E1100–E1107.
15. **Paroder V, Nicola JP, Ginter CS, Carrasco N.** The iodide-transport-defect-causing mutation R124H: A δ-amino group at position 124 is critical for maturation and trafficking of the Na+/I- symporter. *J Cell Sci*. 2013;126:3305–3313.
16. **Li W, Nicola JP, Amzel LM, Carrasco N.** Asn441 plays a key role in folding and function of the Na+/I- symporter (NIS). *FASEB J*. 2013;27:3229–3238.
17. **Paroder-Belenitsky M, Maestas MJ, Dohán O, et al.** Mechanism of anion selectivity and stoichiometry of the Na+/I- symporter (NIS). *Proc Natl Acad Sci U S A*. 2011;108:17933–17938.
18. **De La Vieja A, Ginter CS, Carrasco N.** The Q267E mutation in the sodium/iodide symporter (NIS) causes congenital iodide transport defect (ITD) by decreasing the NIS turnover number. *J Cell Sci*. 2004;117:677–687.
19. **De la Vieja A, Reed MD, Ginter CS, Carrasco N.** Amino acid residues in transmembrane segment IX of the Na+/I- symporter play a role in its Na+ dependence and are critical for transport activity. *J Biol Chem*. 2007;282:25290–25298.
20. **Reed-Tsur MD, De la Vieja A, Ginter CS, Carrasco N.** Molecular characterization of V59E NIS, a Na+/I- symporter mutant that causes congenital I- transport defect. *Endocrinology*. 2008;149:3077–3084.
21. **Faham S, Watanabe A, Besserer GM, et al.** The crystal structure of a sodium galactose transporter reveals mechanistic insights into Na+/sugar symport. *Science*. 2008;321:810–814.
22. **Eswar N, Webb B, Marti-Renom MA, et al.** Comparative protein structure modeling using modeller. *Curr Protoc Bioinformatics*. 2006;Chapter 5:Unit 5.6.
23. **Nicola JP, Nazar M, Mascanfroni ID, Pellizas CG, Masini-Repiso AM.** NF-kappaB p65 subunit mediates lipopolysaccharide-induced Na(+)/I(-) symporter gene expression by involving functional interaction with the paired domain transcription factor Pax8. *Mol Endocrinol*. 2010;24:1846–1862.
24. **Nazar M, Nicola JP, Vélez ML, Pellizas CG, Masini-Repiso AM.** Thyroid peroxidase gene expression is induced by lipopolysaccharide involving nuclear factor (NF)-κB p65 subunit phosphorylation. *Endocrinology*. 2012;153:6114–6125.
25. **Paroder V, Spencer SR, Paroder M, et al.** Na(+)/monocarboxylate transport (SMCT) protein expression correlates with survival in colon cancer: Molecular characterization of SMCT. *Proc Natl Acad Sci U S A*. 2006;103:7270–7275.
26. **Purtell K, Paroder-Belenitsky M, Reyna-Neyra A, et al.** The KCNQ1-KCNE2 K+ channel is required for adequate thyroid I- uptake. *Faseb J*. 2012;26:3252–3259.
27. **Serrano-Nascimento C, da Silva Teixeira S, Nicola JP, Nachbar RT, Masini-Repiso AM, Nunes MT.** The Acute inhibitory effect of iodide excess on sodium/iodide symporter expression and activity involves the pi3k/akt signaling pathway. *Endocrinology*. 2014;155:1145–1156.
28. **De la Vieja A, Ginter CS, Carrasco N.** Molecular analysis of a congenital iodide transport defect: G543E impairs maturation and trafficking of the Na+/I- symporter. *Mol Endocrinol*. 2005;19:2847–2858.
29. **Dohán O, Portulano C, Basquin C, Reyna-Neyra A, Amzel LM, Carrasco N.** The Na+/I symporter (NIS) mediates electroneutral active transport of the environmental pollutant perchlorate. *Proc Natl Acad Sci U S A*. 2007;104:20250–20255.
30. **Riedel C, Levy O, Carrasco N.** Post-transcriptional regulation of the sodium/iodide symporter by thyrotropin. *J Biol Chem*. 2001;276:21458–21463.
31. **Kaminsky SM, Levy O, Salvador C, Dai G, Carrasco N.** Na(+)-I- symport activity is present in membrane vesicles from thyrotropin-deprived non-I(-)-transporting cultured thyroid cells. *Proc Natl Acad Sci U S A*. 1994;91:3789–3793.
32. **Rhoden KJ, Cianchetta S, Stivani V, Portulano C, Galietta LJ,**

Romeo G. Cell-based imaging of sodium iodide symporter activity with the yellow fluorescent protein variant YFP-H148Q/I152L. *Am J Physiol Cell Physiol*. 2007;292:C814–C823.
33. **Nicola JP, Carrasco N, Amzel LM.** Physiological sodium concentrations enhance the iodide affinity of the Na(+)/I(-) symporter. *Nat Commun*. 2014;5:3948.
34. **Brent GA.** Mechanisms of thyroid hormone action. *J Clin Invest*. 2012;122:3035–3043.
35. **Kosugi S, Sato Y, Matsuda A, et al.** High prevalence of T354P sodium/iodide symporter gene mutation in Japanese patients with iodide transport defect who have heterogeneous clinical pictures. *J Clin Endocrinol Metab*. 1998;83:4123–4129.
36. **Vulsma T, Rammeloo JA, Gons MH, de Vijlder JJ.** The role of serum thyroglobulin concentration and thyroid ultrasound imaging in the detection of iodide transport defects in infants. *Acta Endocrinol (Copenh)*. 1991;124:405–410.
37. **Martín MG, Turk E, Lostao MP, Kerner C, Wright EM.** Defects in Na+/glucose cotransporter (SGLT1) trafficking and function cause glucose-galactose malabsorption. *Nat Genet*. 1996;12:216–220.